

Article

Study on Shear Mechanical Properties and Fracture Evolution Mechanism of Irregular Serrated Rock Discontinuities

Xinpeng Li ¹, Dong Wang ^{1,2,*}, Yujing Jiang ^{1,2,3}, Hengjie Luan ^{1,2,4}, Sunhao Zhang ³, Changsheng Wang ² and Jiankang Liu ^{1,2}

¹ College of Energy and Mining Engineering, Shandong University of Science and Technology, Qingdao 266590, China

² State Key Laboratory of Mining Disaster Prevention and Control Co-Founded by Shandong Province and the Ministry of Science and Technology, Shandong University of Science and Technology, Qingdao 266590, China

³ School of Engineering, Nagasaki University, Nagasaki 852-8521, Japan

⁴ Inner Mongolia Shanghaimiao Mining Co., Ltd., Ordos 016299, China

* Correspondence: wdwinter@163.com

Abstract: To analyze the shear characteristics and mesoscopic failure mechanism of irregular serrated rock discontinuities, a great deal of interview samples of irregular serrated structures were made by 3D printing technology, and laboratory shear tests were carried out on them under different normal stresses. At the same time, PFC numerical simulation software is used to establish relevant models to study the evolution of microcracks and the distribution characteristics of the force chain on the rock discontinuity during the shear process. The results show that the shear mechanical properties of irregular serrated rock discontinuities are affected by normal stress, undulating angle, and undulating height. The shear strength increases with the increase of normal stress and undulating height, and decreases with the increase of undulating angle. The numerical simulation results show that the irregular structural surface cracks under different undulation angles, which first start at the near force end serration root on both sides and further evolve to the adjacent serrations, while the irregular structural surface cracks under different undulation heights, which first start at the serration root with the lowest height and expand to the adjacent serrations. At the same time, the number of cracks increases with the increase of normal stress and the force chain is mainly distributed near the sawtooth surface. The force chain is more concentrated near the near force end sawtooth and at the tip and root of the rest of the sawtooth. At the same time, the direction of the force chain is approximately perpendicular to the force surface of the sawtooth. The research results are helpful in further understanding the shear mechanical properties and differences of irregular serrated rock discontinuities.

Keywords: sawtooth; rock discontinuity; microcrack; force chain; shear properties



Citation: Li, X.; Wang, D.; Jiang, Y.; Luan, H.; Zhang, S.; Wang, C.; Liu, J. Study on Shear Mechanical Properties and Fracture Evolution Mechanism of Irregular Serrated Rock Discontinuities. *Appl. Sci.* **2023**, *13*, 2444. <https://doi.org/10.3390/app13042444>

Academic Editor: Arcady Dyskin

Received: 26 January 2023

Revised: 11 February 2023

Accepted: 11 February 2023

Published: 14 February 2023



Copyright: © 2023 by the authors. Licensee MDPI, Basel, Switzerland. This article is an open access article distributed under the terms and conditions of the Creative Commons Attribution (CC BY) license (<https://creativecommons.org/licenses/by/4.0/>).

1. Introduction

Due to its geological structure, there are a lot of rock discontinuities in rock mass. The existence of rock discontinuity affects the shear strength and deformation characteristics of rock mass, and then affects the stability of rock mass [1–4]. Generally, the rock discontinuity of rock mass can be divided into four types according to its geometric shape: straight, wavy, serrated, and stepped [5,6]. Among them, serrated rock discontinuity is a typical form of a rock discontinuity, which is widely developed in natural slopes of hard rock mass and excavation slopes, and has an obvious irregular serrated shape, as shown in Figure 1 [7].

At present, some achievements have been made in the research on the shear mechanical properties of rock discontinuities. Li et al. [8,9] studied the effects of shear rates, normal stresses, and undulating angles on the shear mechanical properties of manually poured serrated specimens through shear tests. Zhang et al. [10] proposed a calculation model for shear stiffness of the rock discontinuity by carrying out shear tests under different

normal stresses on the serrated rock discontinuity and analyzing the experimental data. Shen [11] and Cheng [12] also carried out shear tests on dentate rock discontinuities under different normal stresses and proposed empirical constitutive relations for shear deformation characteristics of rock discontinuities. Einstein et al. [13] conducted a shear test on sawtooth rock discontinuity made of gypsum and analyzed the phenomenon of climbing and gnawing in the shear process. Ji et al. [14] studied the deformation and failure characteristics and shear strength change rules of non-through serrated rock discontinuities with different rock discontinuity angles under different axial pressures by conducting direct shear tests on samples of artificially cast non-through serrated structures. Seidel et al. [15] found the shear test of the serrated rock discontinuity, analyzed the change of rock discontinuity energy in the shear process, and expounded the relationship between rock discontinuity deformation and normal stress. Zhou et al. [16] conducted shear tests on tooth-shaped specimens with different undulating heights under different normal stress conditions, and found that under the same normal stress conditions, the greater the undulating height, the higher the shear strength. Cheng et al. [17] studied the quantitative relationship between the shear strength parameters of the serrated rock discontinuity and the serrated undulating angle of the rock discontinuity through the indoor direct shear test and expounded the failure characteristics of the regular serrated rock discontinuity.



Figure 1. Natural irregular sawtooth rock discontinuity [7].

The above are all studies on the shear mechanical properties of serrated rock discontinuities through laboratory tests. PFC and other numerical simulation software have been widely recognized by the international rock mechanics community in terms of rock mechanics tests and mesoscopic research [18]. Bahadadini et al. [19] studied the shear behavior and roughness degradation mechanism of rock joints under direct shear test conditions through PFC numerical simulation and experimental methods, and the test results also verified the feasibility of PFC numerical simulation software in rock mechanics tests. Zhou et al. [20] conducted shear rheological numerical simulation on the through and non-through joint models established by PFC software, and analyzed the influence of sample size on the shear mechanical behavior of the model. Zhang et al. [21] established five regular serrated joint models with different undulating angles by using the discrete element numerical method, and studied the shear mechanical properties of joints under creep conditions. Jiang et al. [22] used the discrete element method to establish a new bond contact model and studied the influence of different joint geometry on rock shear behavior. Jiang et al. [23] studied the influence of cyclic load on macro and mesoscopic shear properties of rock joints through PFC particle flow software, mainly considering shear displacement shear stress characteristics, shear displacement normal displacement characteristics, distribution and evolution characteristics of cracks and force chains, and the relationship between crack development and shear stress. Huang et al. [18] studied

the influence of undulating angle and normal stress on shear deformation and strength of serrated discontinuity through PFC simulation. Bahadadini et al. [24] proposed a new method for the formation of a shear box, which was used to establish serrated joint models with different undulating angles for direct shear tests. The test results show that the test results of this method are in good agreement with the traditional empirical model. Yang et al. [25] studied the direct shear behavior and failure mechanism of granite bridges between discontinuous joints by using the plane joint simulation method. Tang et al. [26] established the rock discontinuity calculation model under different sawtooth heights through FLAC numerical simulation software and discussed the stress-strain relationship before and after the peak shear strength of the rock discontinuity. Xia et al. [27] generated a rough joint profile in the PFC software and simulated its shear properties to observe the macro failure process of joints from a mesoscopic perspective. Liu et al. [28] conducted indoor direct shear tests and PFC2D numerical simulation tests on the through serrated (wavy) rock mass rock discontinuity containing first-order (second-order) undulations and studied its shear mechanical properties. R.H. Cao et al. [29] studied the peak shear strength and failure process of rock specimens with multiple joints. In general, most scholars have taken a direct shear test and numerical simulation of microparticle flow as the research means of rock discontinuity and achieved remarkable results.

However, all of the above scholars have studied the regular serrated rock discontinuities. However, most of the serrated rock discontinuities in nature are irregular and uneven. Studying the irregular serrated rock discontinuities is an important supplement to the research on the shear characteristics of rock discontinuities, and provides a useful reference for slope treatment. For this reason, the irregular serrated rock discontinuity is made by 3D printing technology, and its shear mechanical properties and fracture evolution mechanism are studied by indoor shear tests and numerical simulation software. The relevant results can provide a reference for subsequent research on the shear properties of irregular serrated rock discontinuities.

2. Laboratory Direct Shear Test

2.1. Specimen Preparation

In this paper, the influence of the undulation angle and height of the jagged rock discontinuity on the shear mechanical properties of rock discontinuity is especially considered in the test. Undulation angle and undulation height are both important roughness factors affecting irregular serrated rock discontinuities, and we request that only one factor changes in each series of tests [30]. Therefore, according to previous studies [18,21,26], we designed the height of the sawteeth to be fixed and the angle of the sawteeth to be 40°, 50°, and 60°. Its shape is shown in Figure 2a (the value marked in the figure is the angle or height of sawtooth undulation). We designed the angle of the sawteeth to be fixed. The height of fluctuation is 6 mm, 8 mm, and 10 mm, and its shape is shown in Figure 2b. The number of sawteeth on rock discontinuities with different undulating angles is the same, and the number of sawteeth on rock discontinuities with different undulating heights is the same, to achieve the purpose of studying the influence of different undulating angles and heights on the shear strength of irregular sawtooth rock discontinuities. To ensure that the size of the rock discontinuity meets the size of the shear box of the shear tester, the total size of the specimen is 100 mm × 100 mm × 100 mm (length × width × height). During the experiment, the irregular sawtooth rock discontinuity is composed of two half-test blocks, which are consistent with each other up and down. The rock discontinuity is located in the central part of the whole sample, to facilitate the study of the change of its shear characteristics.

Because it is difficult to collect the original rock discontinuity in the field, even if the rock discontinuity can be collected, it cannot guarantee that the samples with different block structures have the same morphological characteristics. 3D printing technology has been paid more and more attention to and applied in mining and geotechnical fields, providing a new technical means for the experimental research of rock discontinuity and fractured

rock mass. The deformation characteristics, failure characteristics, and crack initiation and expansion of the 3D printing model are similar to rocks, and the test results of this method have good stability and consistency [31–33]. For this reason, this paper uses AutoCAD software to build the 3D model required for this experiment and slices the model. Finally, the 3D model is imported into the printer. The working principle of the 3D printing process and 3D printer are shown in Figure 2 [33]. Finally, a large number of interview pieces with irregular jagged structures were produced based on 3D printing technology, as shown in Figure 3. At the same time, the mechanical properties of the materials of the printing specimens were tested, and the compressive strength and elastic modulus of the printed model were measured to be 10.12 MPa and 18.34 GPa.

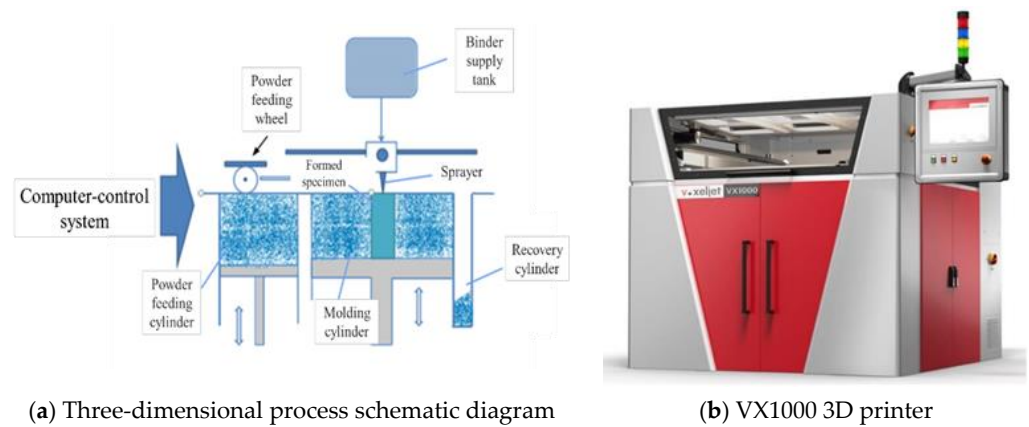


Figure 2. Working principle and equipment of 3D printing process [33].

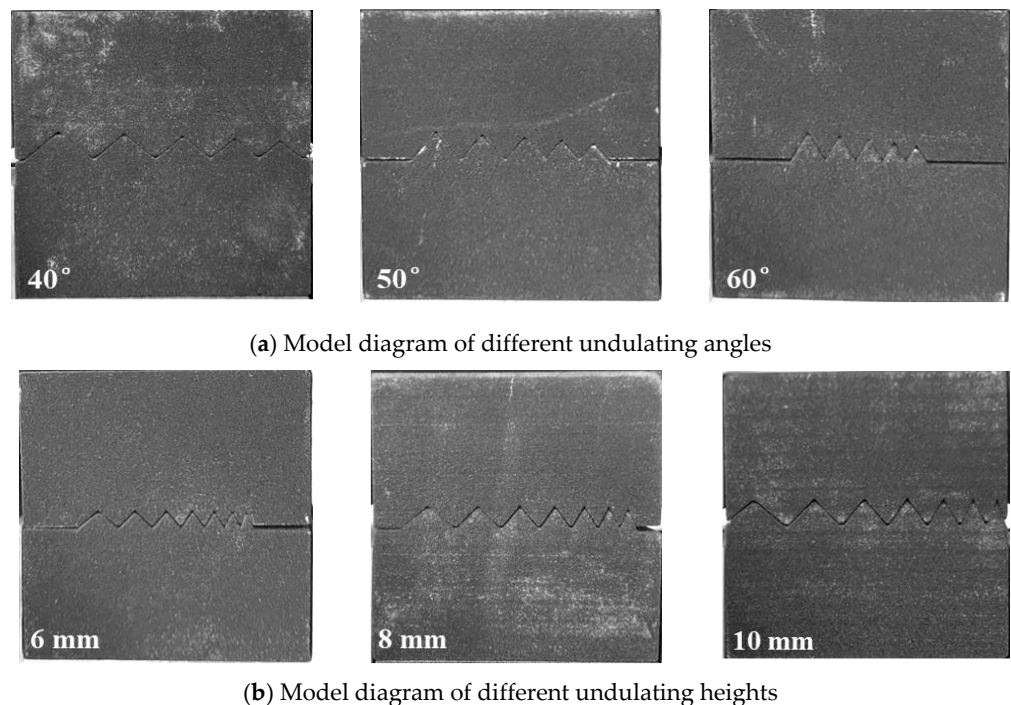


Figure 3. Model diagram of different undulating angles and height.

2.2. Test Plan

In addition to the above effects of the angle and height of relief, the effect of normal stress on the shear mechanical properties of the irregular sawtooth plane is also fully considered in this experiment. Considering the small normal stress on the surface of rock slope, this paper selects 50%, 30%, and 10% (0.5σ , 0.3σ , 0.1σ) as uniaxial compression

strength in reference to the relevant literature [10] to study the influence of different normal stresses on the shear mechanical properties of the irregular sawtooth rock discontinuity. To sum up, the test scheme is shown in Table 1.

Table 1. Test Scheme.

Serial No	Normal Stress/MPa	Undulating Height/mm	Undulating Angle/°	Research Objective
1	2	6–10	40	Effect of normal stress
2	3	6–10	40	
3	4	6–10	40	
4	3	6–10	40	Effect of undulating height
5	3	6–10	50	
6	3	6–10	60	
7	3	6	40–70	Effect of undulating angle
8	3	8	40–70	
9	3	10	40–70	

2.3. Test Device and Test Procedure

The Rjst-616 rock discontinuity shear tester as shown in Figure 4 was adopted in this test scheme. The maximum output force of the normal and tangential loading cylinders of the device are 200 kN and 300 kN, respectively, and the force and displacement control modes can be adopted for both normal and tangential loading. The accuracy of the loading force value and displacement measurement is $\pm 0.5\%$ F.S. During the test, the force and displacement in the normal and shear directions can be automatically collected with a sampling frequency of 10 Hz, and the corresponding curves can be displayed in real time. The detailed parameters of the shear tester are shown in the paper [34].

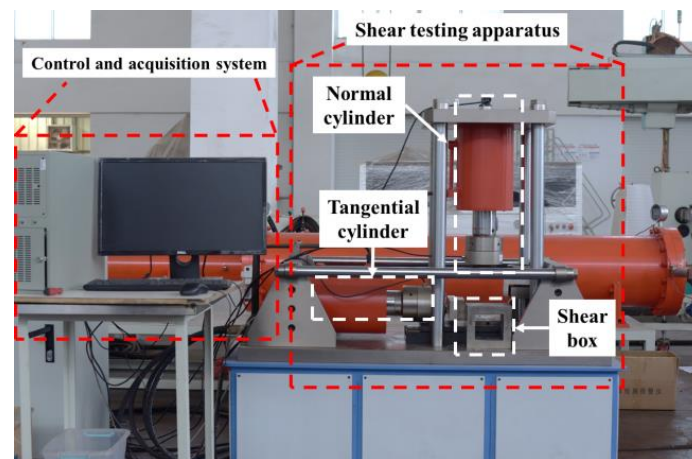


Figure 4. Test equipment diagram.

At the beginning of the test, the normal stress was applied to the shear box above the shear box at the loading speed of 0.1 mm/min and maintained through the displacement control loading mode in the normal direction. Then, in the shearing direction, the upper part of the shear box is fixed, and the shear head applies the shear force at the lower part of the shear box at a speed of 0.5 mm/min through the displacement-controlled loading mode until the specimen is damaged, and the shear test curves and test data of the irregular sawtooth rock discontinuity under different working conditions are obtained.

3. Test Results and Analysis

3.1. Shear Characteristics Analysis

The shear displacements and shear stress curves of the displacements meet expectations, and can better reflect the shear characteristics of irregular sawtooth displacements

under different influencing factors (normal stress, undulating angle, undulating height). According to the test results, the shear displacement–shear stress curve of the rock discontinuity is shown in Figure 5.

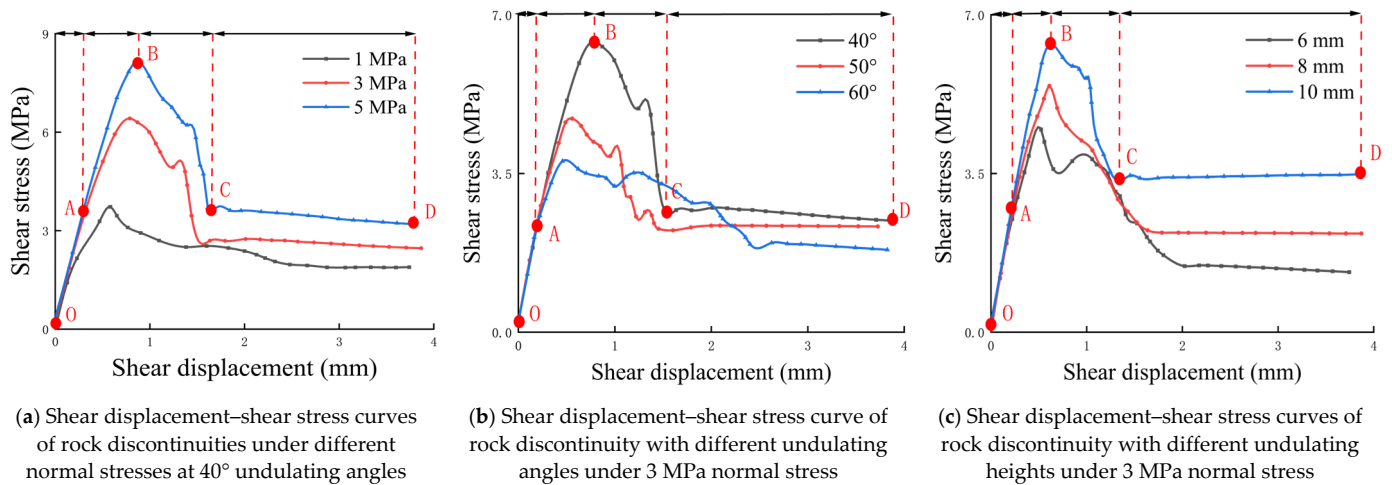


Figure 5. Shear displacement–shear stress curve of rock discontinuity.

3.1.1. The Influence of Normal Stress

It can be seen from Figure 5a that the shear stress–shear displacement curve can be roughly divided into four stages. ① The initial linear stage (OA): In this stage, the shear stress increases along the line with the increase of shear displacement, the slope of the curve is fixed, the shear stiffness is constant, and the slope of the curve is basically the same under different normal stresses. ② Pre-peak nonlinear stage (AB): In this stage, from the end of the OA segment to the peak strength point, the shear stress no longer presents a linear increase with the increase of shear displacement, but a nonlinear increase and the slope of the curve becomes smaller. This is because tiny cracks start to sprout inside the sawtooth and expand rapidly, leading to smaller shear stiffness until macroscopic cracks appear. When macroscopic cracks appear in the sawtooth, the rock discontinuity reaches peak strength. At the same time, it can be found that the shear stiffness is related to the normal stress, and the larger the normal stress is, the larger the shear stiffness is. ③ post-peak softening stage (BC): the curve at this stage shows that the shear stress decreases with the increase of shear displacement, which is the first failure of the near end of the sawtooth, and the shear force is transferred to the far end. The sawtooth is constantly nipped, the resistance of the sawtooth to the shear force is weakened, and the curve is softened. ④ Residual strength stage (CD): at this stage, the shear stress does not change significantly with the increase of shear displacement. At this stage, all the sawteeth are nipped, but the rock discontinuity still bears a certain shear stress. The shear strength at this stage is provided by the friction effect of the sawtooth plane after nibbling. The residual strength is related to normal stress. The larger the normal stress is, the greater the residual strength will be.

3.1.2. The Influence of Different Undulating Angles

Figure 5b shows the shear stress–shear displacement curve under the influence of different angles. The curve can also be divided into four stages. ① The initial linear stage (OA): In this stage, the shear stress increases linearly with the increase of shear displacement, and the slope of the curve under different undulating angles is the same, and the shear stiffness is the same. ② Pre-peak nonlinear stage (AB): The slope of the curve in this stage is related to the angle of sawtooth relief. The smaller the angle of relief, the larger the slope of the curve, the larger the shear stiffness, and the increase of shear stress with the increase of shear displacement; ③ Post-peak softening stage (BC): With the increase of

shear displacement, the shear stress gradually decreases, and the reduction rate is related to the magnitude of the undulating angle; the larger the undulating angle, the smaller the reduction rate; ④ Residual strength stage (CD): After the saw-tooth nibbling failure, the rock discontinuity is still under shear stress. Currently, the shear strength enters a constant state, and the residual strength under different undulating angles is the same.

3.1.3. The Influence of Different Undulating Heights

As can be seen from Figure 5c, the shear stress–shear displacement curve under the influence of different undulating heights can also be divided into four stages. ① The initial linear stage (OA): In this stage, the shear stress increases linearly with the increase of shear displacement, the slope of the curve is fixed, and the shear stiffness is constant. It shows that the shear stiffness has nothing to do with the height of the jagged teeth. ② Pre-peak nonlinear stage (AB): This stage starts from the end point of the initial linear stage to the peak point of the curve. At this stage, with the increase of shear displacement, the shear stress increases slowly, the slope of the curve becomes smaller, and the shear stiffness becomes smaller. Furthermore, the shear stiffness is related to the height of relief. The larger the height of the relief is, the larger the shear stiffness is. ③ Post-peak softening stage: Currently, the shear stress reaches its peak, and with the continuous increase of shear displacement, the shear stress begins to decline. Obvious brittle failure is found on the rock discontinuity, and most of this failure first occurs at the root of the near force end of the sawtooth on both sides and is rapidly transmitted to the rest of the sawtooth, accompanied by an obvious brittle sound, which shows the softening of shear stress on the curve. ④ Residual strength stage (CD): With sawtooth failure and shear stress fall, the rock discontinuity still bears a certain shear stress, and the shear stress is mainly provided by the broken sawtooth friction.

3.2. Analysis of Influencing Factors and Failure Characteristics of Shear Strength

3.2.1. Effect of Normal Stress on Shear Strength

As can be seen from Figure 6, the shear strength of the rock discontinuity is jointly affected by normal stress, undulating angle, and undulating height. When other factors remain unchanged, the shear strength of the rock discontinuity increases with the increase of normal stress. The shear strength decreases with the increase of the angle of relief when the height of relief of the rock discontinuity remains constant. The shear strength of the rock discontinuity is also affected by the height of the relief of the rock discontinuity. The shear strength increases with the increase of the height of the relief.

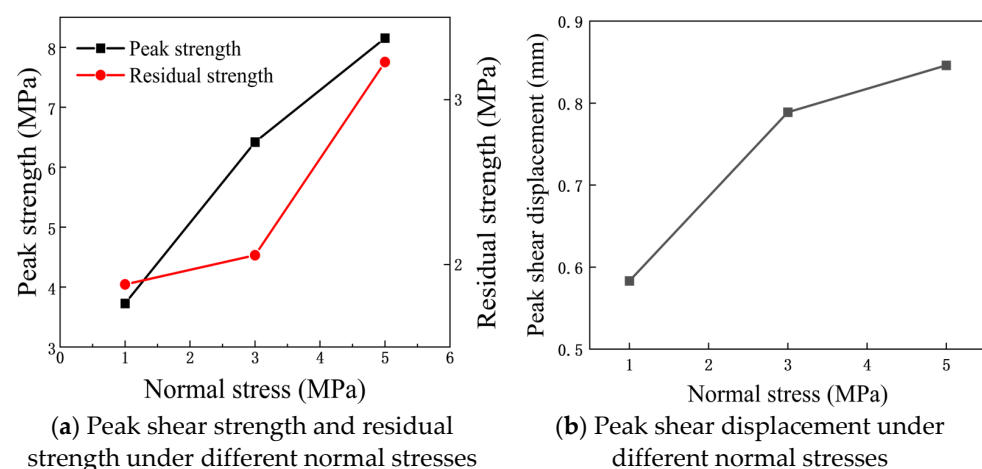


Figure 6. Shear strength curves under different normal stresses at 40° undulating angles.

3.2.2. Effect of Undulating Angle on Shear Strength

As can be seen from Figure 7, under the condition that the normal stress is 3 MPa, both the shear peak and residual strength of the rock discontinuity decrease with the increase of the undulating angle. The shear peaks of the rock discontinuity at 40°, 50°, and 60° are 6.42 MPa, 4.7 MPa, and 3.77 MPa, respectively, and the shear peaks are the largest when the undulating angle is 40°. When the undulating angle increases from 40° to 60°, the residual strength of the rock discontinuity decreases from 2.48 MPa to 1.84 MPa. At the same time, it can be seen from Figure 7 that the peak shear displacement of the rock discontinuity decreases approximately linearly with the increase of the undulating angle. When the undulating angle increases from 40° to 60°, the peak shear displacement decreases from 0.789 mm to 0.457 mm.

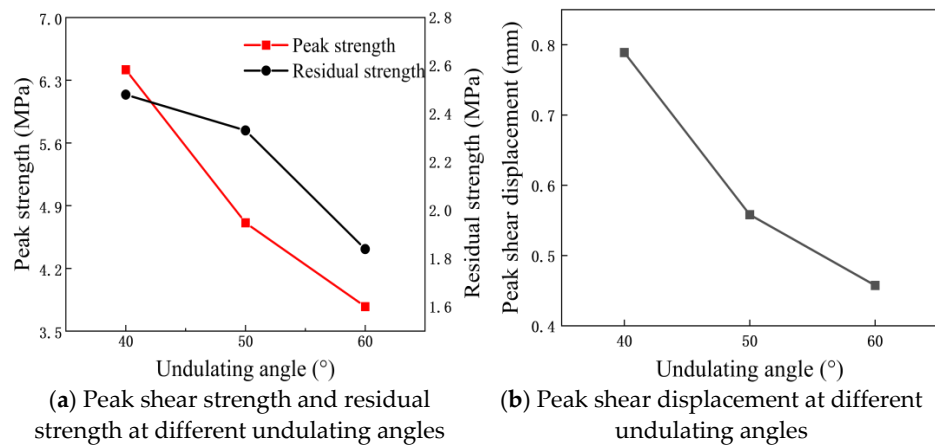


Figure 7. Shear strength curves under the influence of different undulating angles.

3.2.3. Effect of Undulating Height on Shear Strength

As can be seen from Figure 8, under the condition that the normal stress is 3 MPa, the shear peak and residual strength of the rock discontinuity increase approximately linearly with the increase of the undulating height. When the undulating height increases from 6 mm to 10 mm, the shear peak value increases from 4.47 MPa to 6.34 MPa, and the residual strength increases from 1.35 MPa to 3.33 MPa. Meanwhile, the peak shear displacement of rock discontinuity increases with the increase of undulating height. When the undulating height increases from 6 mm to 10 mm, the peak shear displacement increases from 0.523 mm to 0.62 mm. However, the peak shear displacements at 8 mm and 10 mm undulating heights are almost equal, indicating that the peak shear displacements of rock discontinuity show little change when the sawtooth reaches a certain undulating height.

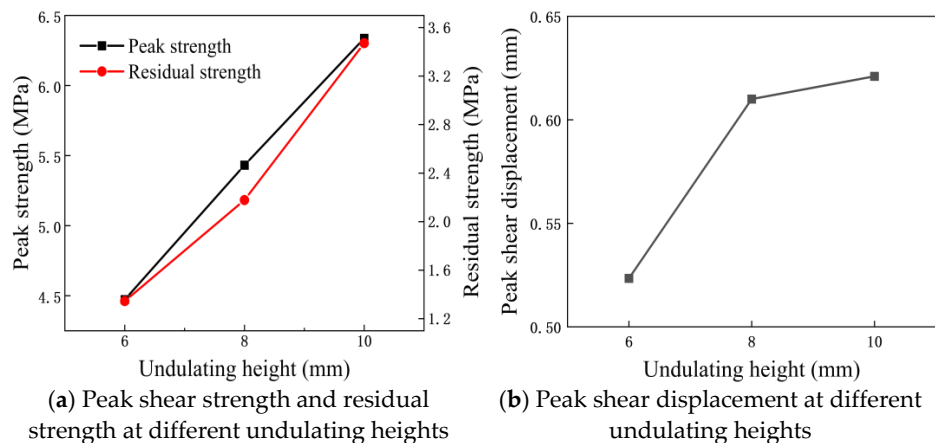


Figure 8. Shear strength curves under the influence of different undulating heights.

3.2.4. Analysis of Shear Failure Characteristics

Figure 9 shows the failure diagram of a shear test at 60° undulating angle and 8 mm undulating height of 3 MPa normal stress. As can be seen from Figure 9, when the saw-tooth of rock discontinuity is damaged, the through damage occurs from the root of the sawtooth. Among them, the rock discontinuity sawteeth at 60° undulation angle were all nibbled from the root of the footer sawteeth, and the fracture direction was almost parallel to the shear direction. This is because under the normal stress of 3 MPa, the rock discontinuities of the upper and lower plates mesh with each other, and the rock discontinuities of the lower plates move to the left under the action of the shear force. However, under the relatively high undulating angle of 60° , due to the fixed height of the teeth, the larger the angle, the narrower the teeth, and the ability of the teeth to resist the shear action is weak, so the teeth are nipped off before climbing occurs. Except for the large sawtooth on the right side of the footer, all the other sawteeth were damaged at the height of 8 mm fluctuation. This is because when the angle of relief is fixed, the width of sawtooth decreases with the increase of the height of relief. Under the action of shear force, after the sawtooth with the smallest width on the left side was first nibbled, the shear force gradually transferred to the adjacent sawtooth, and with the increase of shear displacement, the small sawtooth that was damaged first turned over. Finally, except for the sawtooth with the largest width on the right side, all the other sawteeth were nibbled.

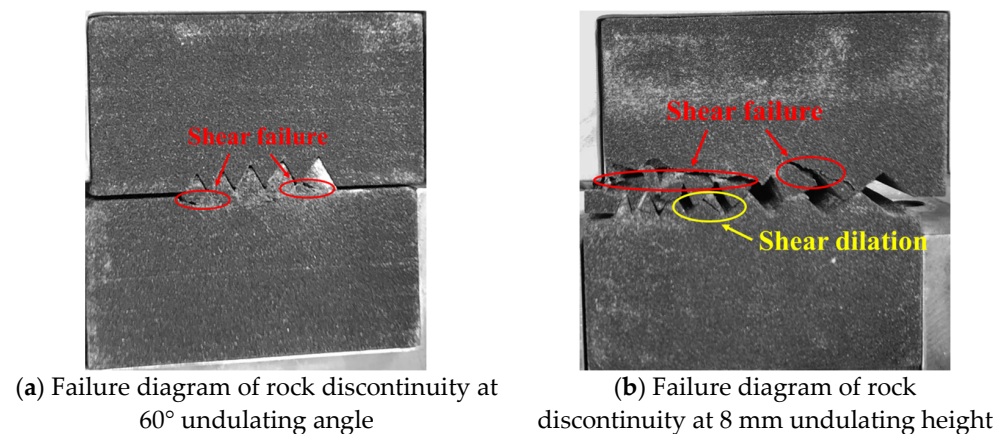


Figure 9. Shear test failure diagram.

4. PFC2D Numerical Simulation of Granular Flow

To further reveal the damage evolution process and crack propagation mechanism of irregular sawtooth rock discontinuity from the mesoscopic perspective, a numerical calculation model of the above test conditions was established by using the PFC2D particle flow program on the basis of laboratory direct shear tests. The longitudinal and transverse failure of the model was observed from the distribution of microcracks and contact forces, as well as the stress and displacement in the shear direction and normal direction [35].

4.1. Establishment of PFC Direct Shear Model

A total of 6 walls were built to simulate the shear box, and the size of the shear box was height \times width = 100 mm \times 100 mm. Among them, walls 1, 3, and 4 form the upper shear box, which serves as the loading wall together, while walls 2, 5, and 6 form the lower shear box, which is fixed. Meanwhile, in order to prevent particles from escaping during the loading process, walls 7 and 8 are established as wing walls [36], so as to ensure the normal conduct of the whole direct shear test.

A total of 14,082 particles were randomly generated within the established shear box, with a particle density of 2480 kg/m³, particle radius of 0.4~0.5 mm, conforming to a uniform distribution, and a porosity of 0.1. The parallel bond model was used as the mesoscopic constitutive model, the smooth joint contact model [36] was used to simulate

the irregular zigzag plane, and the discrete fracture network (DFN) was used to create the through-through plane. The direct shear model of rock joints shown in Figure 10 (40° undulating angle model under normal stress of 1 MPa) was built. The smooth joint contact model was applied to the particles within the range of 0.5 mm.

The model boundary conditions applied in the numerical simulation are the same as those in the laboratory test as follows: the horizontal movement of the lower specimen was restricted, that is, the horizontal movement of #2, #5, and #6. The normal velocity of wall #1 was controlled by the servo function, and the constant normal stress was applied to the top of the specimen. A horizontal velocity of 0.02 mm/s was set for walls #1, #3, #4, and #7 to realize the application of shear load.

Laboratory tests can not directly obtain granular contact modulus, cohesion, tensile strength, and other mesoscopic parameters, so it is very important to establish the matching relationship between granular mesoscopic parameters and direct shear macro-mechanical parameters of rock materials. Therefore, combined with the results of the rough joint shear test, the mesoscopic parameters of the specimen were calibrated by the “trial-and-error method [19]”. The simulation results are shown in Figure 11, and the parameters identified are shown in Tables 2 and 3. It can be seen from Figure 11 that the numerical simulation test had a good consistency with the laboratory test results.

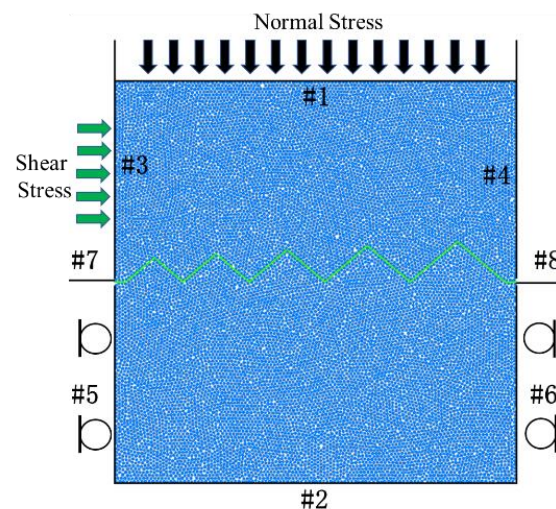


Figure 10. Simulation diagram of specimen with 40° undulating angle.

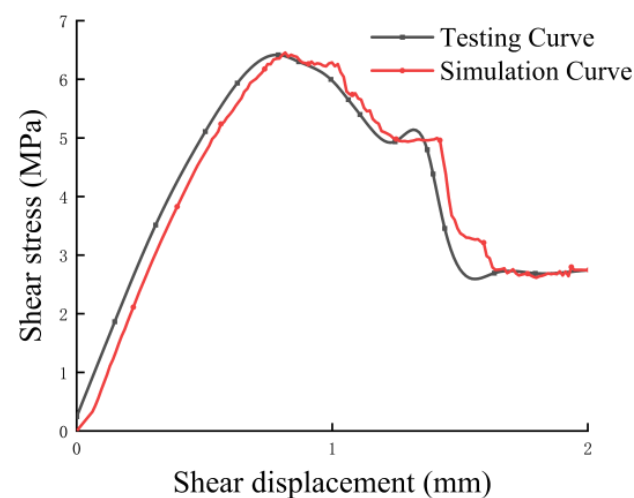


Figure 11. Laboratory direct shear test and PFC simulation curve.

Table 2. Mesoscopic parameters of particle and parallel bonding models.

Spherical Particle	Numerical Value	Parallel Bonding Model	Numerical Value
Elasticity Modulus/GPa	1.50	Elasticity Modulus/GPa	1.50
Stiffness Ratio	0.50	Stiffness Ratio	1.50
Friction Coefficient	0.70	Tensile Strength/MPa	6.70
Maximum Particle Radius/mm	0.50	Shear Strength/MPa	18.1
Maximum And Minimum Particle Radius Ratio	1.25	Friction Angle/°	20
Volume Density/kg·m ⁻³	2480		

Table 3. Mesoscopic parameters of smooth joints model.

Numerical Value	Normal Stiffness/GPa·m ⁻¹	Shear Stiffness/GPa·m ⁻¹	Friction Coefficient	Tensile Strength/MPa	Cohesion/MPa
Number	200	200	0.7	0	0

4.2. Shear Damage Mechanism of Rock Discontinuity under Different Normal Stresses

4.2.1. Characteristics of Microcrack Evolution

Figure 12 shows the microcrack evolution diagram of the irregular sawtooth rock discontinuity under the condition that the undulating angle is 40° and the normal stress is 1 MPa, 3 MPa, and 5 MPa, respectively. The values marked in the figure are shear displacement. The dynamic propagation of microcracks and the variation of particle displacement vector in the irregular sawtooth plane under different normal stresses were studied by analyzing the dynamic variation of microcracks.

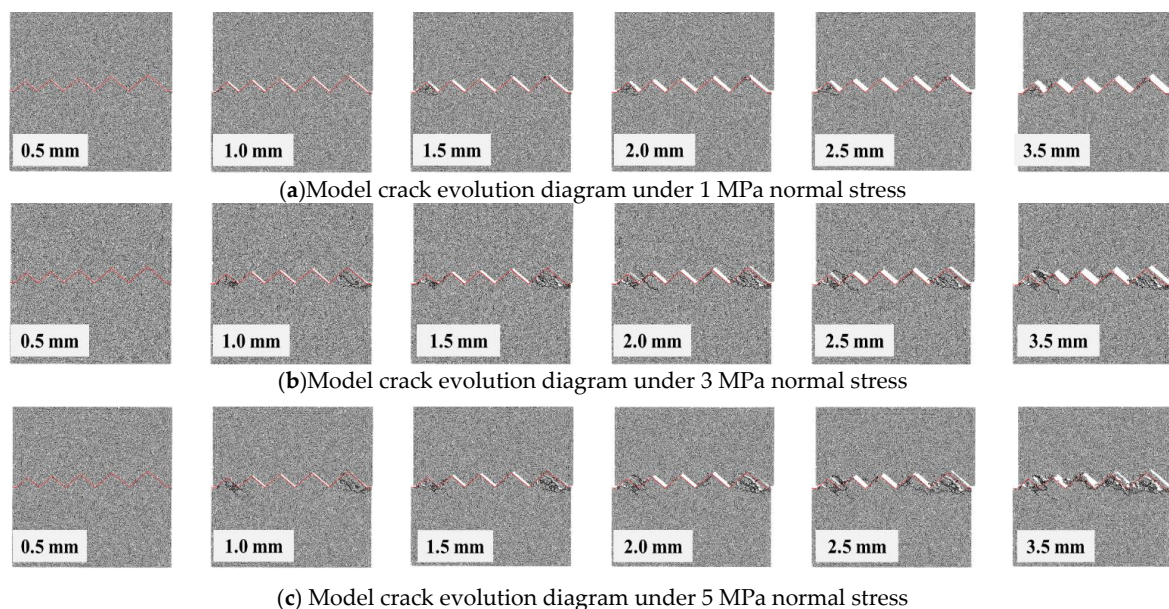


Figure 12. Model crack evolution under different normal stresses.

It can be seen from the results of Figure 12 that, under different normal stresses, the evolution of sawtooth microcracks in the rock discontinuity has great differences. Under the relatively low normal stress of 1 MPa, the upper shear box slides upward along the sawtooth structure with the increase of shear displacement, and there is no crack expansion and the number of cracks is small. Under the relatively high normal stress of 3 MPa and 5 MPa, it can be observed that there is an obvious increase in the number of cracks and the expansion of cracks. This is because the increase of normal stress increases the resistance to the relative movement of particles at the interface, which makes the bonding between

particles at the interface easier to break under high-normal stress [37]. At the same time, cracks first germinate at the near-force sawtooth on the left and right sides. With the continuous increase of shear displacement, a penetrating crack occurs at the near-force sawtooth on both sides, and the upper and lower teeth of the near-force sawtooth on the left side chew each other. The lower sawtooth of the right near force end was nibbled by the upper sawtooth, resulting in obvious thorough damage at the root of the sawtooth. After the near-force end of the sawtooth was nibbled, the crack gradually expanded to the middle of the model.

4.2.2. Distribution Characteristics of Force Chains

The force chain is the transmission path of the external load in granular material at the mesoscale, and it is the bridge between macroscopic stress and microscopic intergranular force. In other words, the size and direction of force chain are determined by the intergranular force, and also determine the macroscopic mechanical properties of the system. The thickness of force chain reflects the size of force, the black line represents the rock discontinuity, and the direction of force chain represents the direction of force. The force chain consists of strong chain and weak chain, and the strong chain and the weak chain interlace each other, forming a complex force chain network. The strong chain mainly plays the role of supporting load and determines the bearing characteristics of the particle system [38].

Figure 13 shows the distribution of force chains of the model when failure occurs under different normal stresses. It can be seen from Figure 13 that with the increase of shear displacement, the distribution of contact forces on the sawtooth surface is consistent with the propagation of microcracks on the structure surface, and the number of strong chains increases significantly with the increase of normal stress. Under the relatively high normal stress of 3 MPa and 5 MPa, the initial shear force chain is mainly concentrated in the near force end of the left and right sawteeth and the tooth tips of other sawteeth. With the increase of shear displacement, after the crack passes through, the left and right sawteeth are nibbled, and the force chain is transferred to the next adjacent sawtooth. The nibbled sawtooth is no longer distributed in the distribution of the strong chain, and the strong chain is mainly distributed in the adjacent sawtooth on the left.

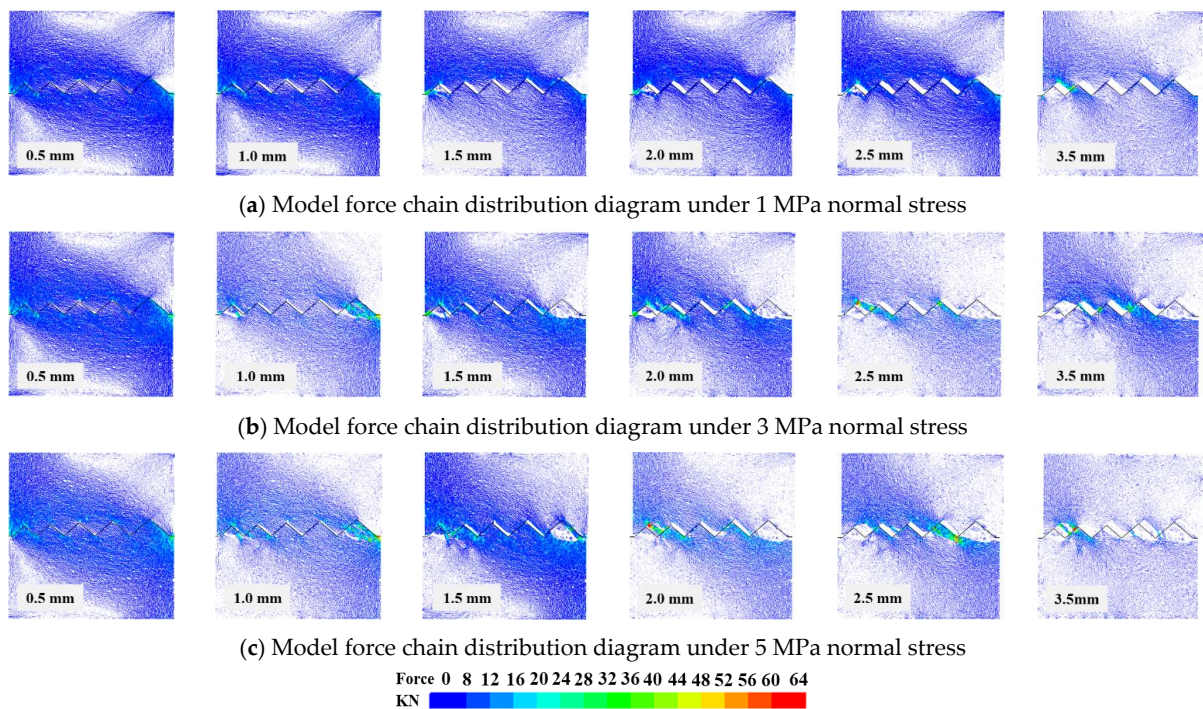


Figure 13. Model force chain distribution under different normal stresses.

4.3. Shear Damage Mechanism of Rock Discontinuity under Different Undulating Angles

4.3.1. Characteristics of Microcrack Evolution

Figure 14 shows the microcrack evolution diagram of the irregular sawtooth rock discontinuity under the normal stress of 3 MPa and the undulating angles of 40° , 50° , and 60° . As can be seen from the results of Figure 14, under different undulating angles, the growth of sawtooth microcracks on the rock discontinuity has great differences, but all of them are concentrated near the sawtooth. Under the relatively small undulating angle of 40° , the cracks first initiate near the sawtooth root of the near force end on both sides, and the cracks continue to expand until they are connected under the action of shear force. The sawtooth located in the middle of the rock discontinuity basically has no cracks. Under the undulating angle of 50° , cracks still occur first at the near force end of the sawtooth on both sides. With the increase of shear displacement, the through cracks occur at both sides of the sawtooth, and the near force end of the sawtooth on both sides is the first to be nipped, among which the small sawtooth is nipped along the root, while the large sawtooth is fractured at the middle and lower part. At the same time, the number of cracks in other sawteeth also increased significantly. When the shear displacement reached 3.5 mm, almost all the sawteeth were nibbled at the root or at the middle and lower parts. When the undulation angle was 60° , at the initial stage of shear, almost all footer sawtooth roots had cracks initiation, because with the increase of the undulation angle, the width of the sawtooth narrowed due to the constant height of the sawtooth, and the shear resistance weakened. With the increase of shear displacement, the root of the left small sawtooth was first damaged. When the shear displacement reached 3.5 mm, all the sawteeth were nibbled away from the root.

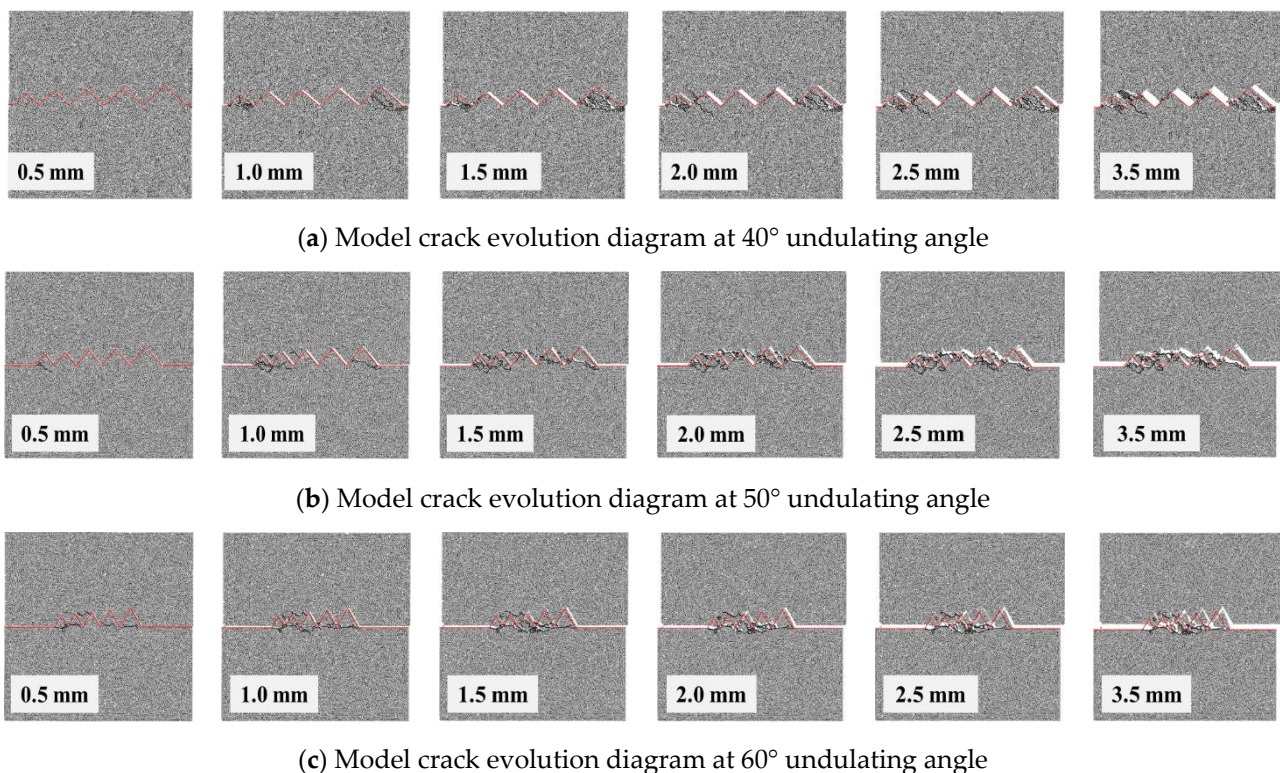


Figure 14. Model crack evolution under different undulating angles.

4.3.2. Distribution Characteristics of Force Chains

Figure 15 shows the distribution diagram of the force chain of the model when the failure occurs at different undulating angles. It can be seen from Figure 15 that, with the increase of shear displacement, the distribution of contact force on the sawtooth surface is consistent with the propagation of microcracks on the structure surface. The strong chains

are mainly concentrated in the vicinity of the near-force sawtooth on both sides, indicating that the shear strength of the rock discontinuity is mainly provided by the large and small sawtooth on both sides, because in the shearing process, the sawtooth on both sides is the first to be nipped and destroyed. With the increase of shear displacement, the force chain is transferred to the middle sawtooth. Under different undulating angles, the force chain size is different. The maximum force chain in the 40° undulating angle model is 48 kN, the maximum force chain in the 50° undulating angle model is 45 kN, and the maximum force chain in the 60° undulating angle model is 41 kN. At the initial stage of shear, the shear stress is small and is mainly affected by normal stress. The direction of the force chain is nearly horizontal. With the increase of the shear stress, the direction of the force chain is approximately perpendicular to the force surface of the sawtooth.

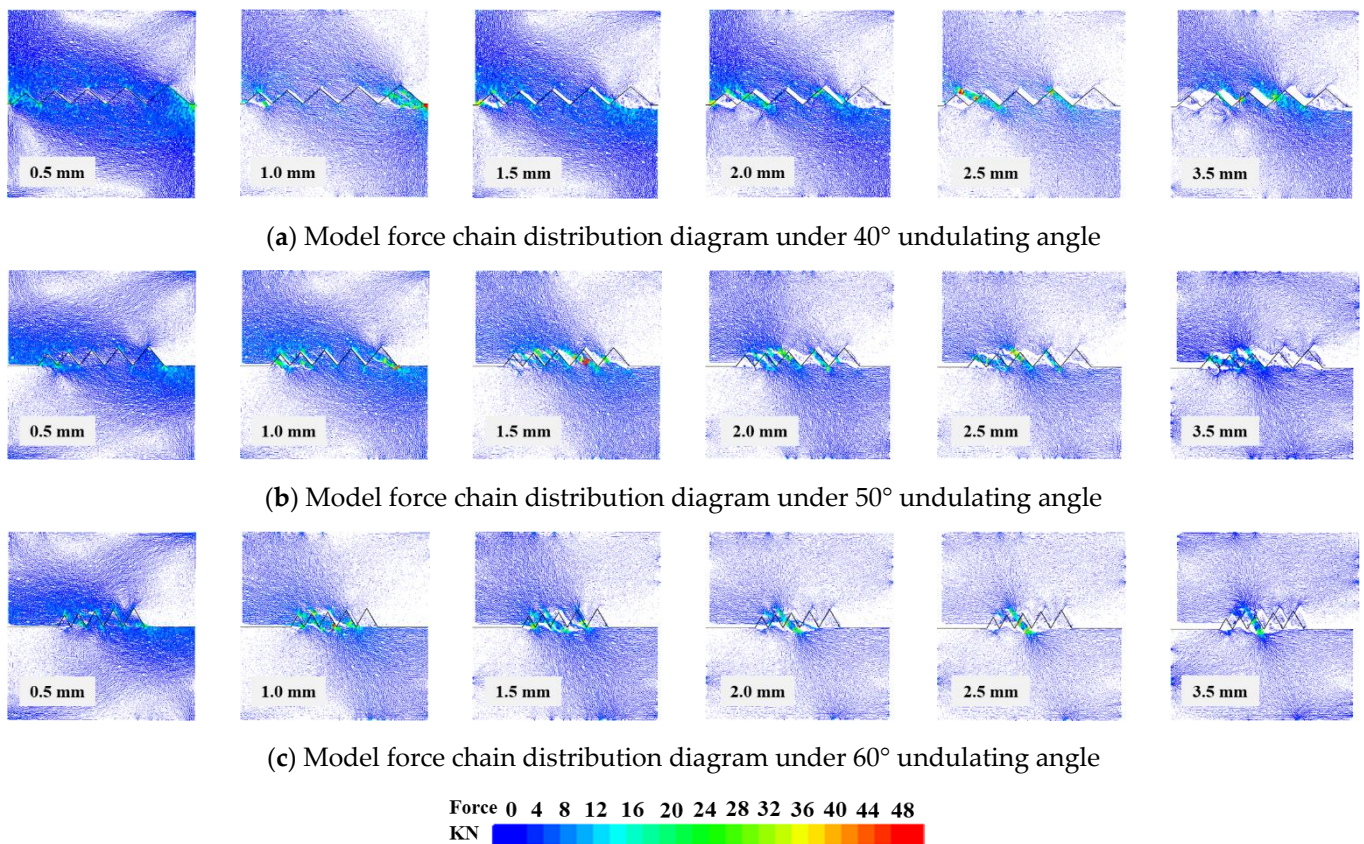


Figure 15. Model force chain distribution under different undulating angles.

4.4. Shear Damage Mechanism of Rock Discontinuity under Different Undulating Heights

4.4.1. Characteristics of Microcrack Evolution

Figure 16 shows the microcrack evolution diagram of the irregular sawtooth rock discontinuity under the normal stress of 1 MPa and the undulating height of 6 mm, 8 mm and 10 mm, respectively. As can be seen from the results of Figure 16, although the undulating heights of the models are different, the cracks all initiate and expand near the sawtooth surface. In the model with relatively small undulating heights of 6 mm and 8 mm, the crack evolution characteristics are very similar. The first initiation of the crack at the right sawtooth root is at a relatively small height near the force end, and with the continuous increase of shear displacement, the sawtooth crack at the near force end constantly evolves toward the adjacent sawtooth. When the shear displacement reaches 3.5 mm, there is no obvious damage except for the left sawtooth. The rest of the sawteeth were chewed off, and the test diagram of the 8 mm sawtooth rock discontinuity is shown in Figure 9b. In the model with a height of 10 mm, the micro-cracks at the initial shear stage

were initiated at the sawtooth near the force end on both sides. With the increase of shear displacement, the cracks gradually evolved inward. When the shear displacement reached 3.5 mm, all the sawteeth had penetrating damage.

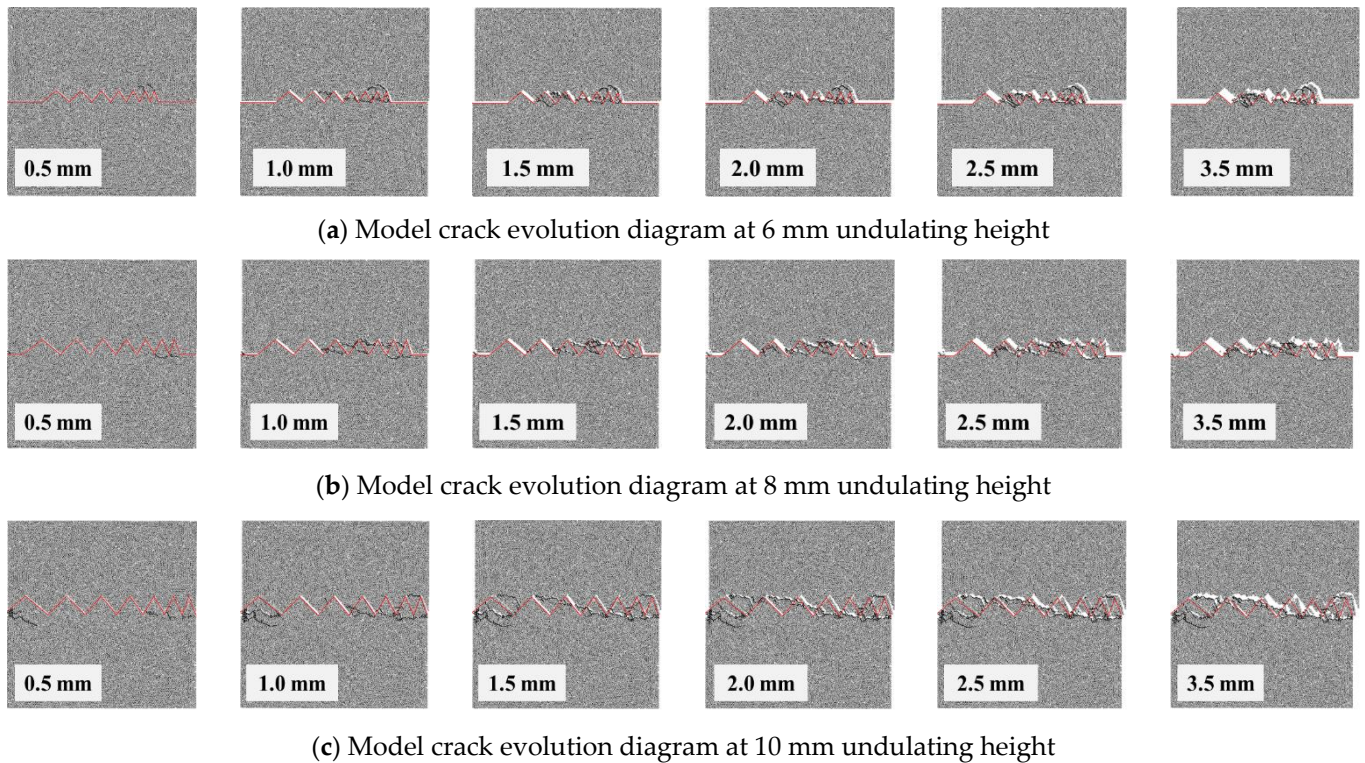


Figure 16. Model crack evolution under different undulating heights.

4.4.2. Distribution Characteristics of Force Chains

Figure 17 shows the distribution diagram of the force chain of the model with different undulating heights. It can be seen from Figure 17 that, with the increase of shear displacement, the distribution of contact force on the sawtooth surface is consistent with the propagation of microcracks on the structure surface. The strength chain is mainly concentrated in the tooth tip and tooth root part of the sawtooth, indicating that the shear strength of the rock discontinuity is mainly provided by the tooth tip and tooth root part of the sawtooth. At the initial shear stage of the 6 mm and 8 mm model, the direction of the force chain is approximately horizontal. With the increase of shear displacement, the direction of the force chain is approximately perpendicular to the force surface of the sawtooth. Due to the irregularity of the sawtooth, the distribution of the force chain on the sawtooth was not uniform. Under the action of shear stress, the sawtooth with weak shear strength was destroyed, and the force chain gradually concentrated on the intact sawtooth end, while the left big sawtooth almost failed to distribute the force chain. At the end of the shear, all the sawteeth except the left big sawtooth were destroyed. However, in the model with an undulating height of 10 mm, the distribution of strong chains of the large sawtooth at the near force end on the left and right sides is concentrated, because the sawtooth at both sides is the first to fail, and the force chain is also gradually concentrated at the remaining sawtooth end. With the continuous increase of shear displacement, all the sawteeth are damaged either from the root of the sawtooth or from the middle of the sawtooth.

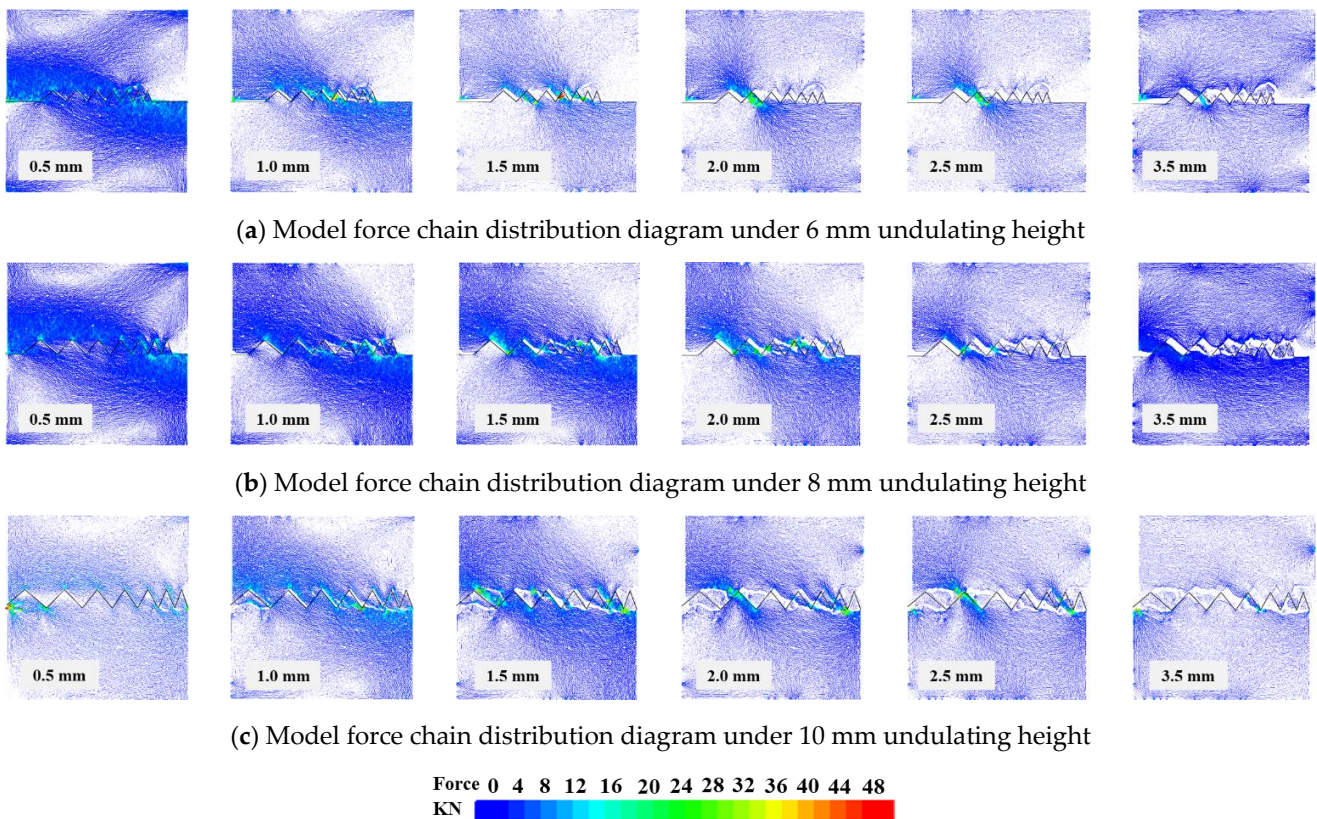


Figure 17. Model force chain distribution under different undulating heights.

5. Conclusions

In this paper, we carried out a series of laboratory shear tests of the irregular serrated rock discontinuities under different normal stresses, different undulating angles, and different undulating heights, and we studied microcosmic crack and force chains by using PFC numerical simulation software. From the test results, the main conclusions can be drawn. The test results are helpful to further understand the shear characteristics of irregular serrated rock discontinuities and provide a reference for engineering rock stability control such as slope management.

(1) The shear stress–shear displacement curve of irregular sawtooth rock discontinuity can be roughly divided into initial linear stage, pre-peak nonlinear stage, post-peak softening stage, and residual stage, and the irregular sawtooth rock discontinuity will also appear in the shear process of climbing, gnawing and climbing, and gnawing failure characteristics.

(2) The shear mechanical properties of the irregular sawtooth plane are affected by normal stress, angle, and height of the sawtooth relief. The peak shear strength and peak shear displacement increase with the increase of normal stress and undulating height, but decrease with the increase of undulating angle.

(3) The number of microcracks is affected by the normal stress, and the larger the normal stress is, the greater the number of microcracks. The micro-cracks on the sawtooth rock discontinuity with different angle of fluctuation mostly originated from the root of the sawtooth near the force end on both sides and gradually expanded to the adjacent sawtooth. The micro-cracks of the sawtooth structure plane with different undulating heights first appear at the root of the sawtooth with a smaller height and gradually expand to the adjacent sawtooth.

(4) In the numerical simulation of PFC, it can be observed that the force chain of the irregular sawtooth rock discontinuity model is concentrated near the sawtooth plane. At the initial shear stage of the model with a relatively small undulating height and angle,

the direction of the force chain is approximately horizontal. With the increase of shear displacement, the direction of the force chain is approximately perpendicular to the force plane of the sawtooth.

Author Contributions: Conceptualization, formal analysis, methodology, writing and editing, D.W. and X.L.; data curation, writing and editing, Y.J. and H.L.; software, S.Z.; review and editing, C.W. and J.L. All authors have read and agreed to the published version of the manuscript.

Funding: This study was funded by the National Natural Science Foundation of China (No. 52204101, 52209141), the Shandong Provincial Natural Science Foundation of China (No. ZR2021QE069, ZR2022QE137), and the open project of the state key laboratory for geomechanics and deep underground engineering in CUMTB (No. SKLGDUEK2023).

Institutional Review Board Statement: Not applicable.

Informed Consent Statement: Not applicable.

Data Availability Statement: Data associated with this research are available and can be obtained by contacting the corresponding author upon reasonable request.

Conflicts of Interest: The authors declare no conflict of interest.

References

1. Wang, C.S.; Liu, R.C.; Jiang, Y.J.; Wang, G.; Luan, H.J. Effect of shear-induced contact area and aperture variations on nonlinear flow behaviors in fractal rock fractures. *J. Rock Mech. Geotech. Eng.* **2022**, *15*, 309–322. [\[CrossRef\]](#)
2. Wang, Y.Y.; Gong, B.; Zhang, Y.J.; Yang, X.Y.; Tang, C.A. Progressive fracture behavior and acoustic emission release of CJBs affected by joint distance ratio. *Mathematics* **2022**, *10*, 4149. [\[CrossRef\]](#)
3. Gong, B.; Wang, Y.Y.; Zhao, T.; Tang, C.A.; Yang, X.Y.; Chen, T.T. AE energy evolution during CJB fracture affected by rock heterogeneity and column irregularity under lateral pressure. *Geomat. Nat. Hazards Risk* **2022**, *13*, 877–907. [\[CrossRef\]](#)
4. Wang, Y.Y.; Gong, B.; Tang, C.A. Numerical investigation on anisotropy and shape effect of mechanical properties of columnar jointed basalts containing transverse joints. *Rock Mech. Rock Eng.* **2022**, *55*, 7191–7222. [\[CrossRef\]](#)
5. Du, S.G.; Lin, H.; Yong, R.; Liu, G.J. Characterization of joint roughness heterogeneity and its application in representative sample investigations. *Rock Mech. Rock Eng.* **2022**, *55*, 3253–3277. [\[CrossRef\]](#)
6. Sun, G.Z. *Foundation of Rock Mass Mechanics*; Science Press: Beijing, China, 1983.
7. Jin, T.W. Study on Shear Characteristics of Regular Dentate Joints. Master's Thesis, Beijing University of Civil Engineering and Architecture, Beijing, China, 2021.
8. Li, H.B.; Feng, H.P.; Liu, B. Study on strength behaviors of rock joints under different shearing deformation velocities. *Chin. J. Rock Mech. Eng.* **2006**, *25*, 2435–2440.
9. Li, H.B.; Liu, B.; Feng, H.P.; Zhang, L.Q. Study of deformability behaviour and failure mechanism by simulating rock joints sample under different loading conditions. *Rock Soil Mech.* **2008**, *29*, 1741–1746.
10. Zhang, Q.Z.; Shen, M.R.; Ding, W.Q. Study on the mechanical properties of rock mass discontinuity under shear condition. *Hydrogeol. Eng. Geol.* **2012**, *39*, 37–42.
11. Shen, M.R.; Zhang, Q.Z. Experimental study of shear deformation characteristics of rock mass discontinuities. *J. Rock Mech. Eng.* **2010**, *29*, 713–719.
12. Cheng, T.; Guo, B.H.; Sun, J.H.; Tian, S.X.; Sun, C.X.; Chen, Y. Establishment of constitutive relation of shear deformation for irregular joints in sandstone. *Rock Soil Mech.* **2022**, *43*, 51–64.
13. Einstein, H.H.; Veneziano, D.; Baecher, G.B.; O'Reilly, K.J. The effect of discontinuity persistence on rock slope stability. *Int. J. Rock Mech. Min. Sci. Geomech. Abstr.* **1983**, *20*, 227–236. [\[CrossRef\]](#)
14. Ji, F.; Yan, X.T.; Zhang, B. Experimental Study on Shear Fracture Evolution Mechanism of Non-penetrating Serrated Structural Surface. *J. Chongqing Jiaotong Univ. Nat. Sci.* **2021**, *40*, 117–123.
15. Seidel, J.P.; Haberfield, C.M. The application of energy principles to the determination of the sliding resistance of rock joints. *Rock Mech. Rock Eng.* **1995**, *28*, 211–226. [\[CrossRef\]](#)
16. Zhou, H.; Meng, F.Z.; Zhang, C.Q.; Yang, F.J.; Lu, J.J. The shear failure characteristic of the structural plane and its application in the study of slip rockburst. *Chin. J. Rock Mech. Eng.* **2015**, *34*, 1729–1738.
17. Cheng, Y.H.; He, D.L.; Qin, J.X.; Yang, J.Y. Effect of sawtooth angle on shear mechanical behavior of structural plane. *Geotech. Geol. Eng.* **2021**, *39*, 4169–4180. [\[CrossRef\]](#)
18. Huang, D.; Huang, R.Q.; Lei, P. Shear deformation and strength of through-going saw-tooth rock discontinuity. *J. China Coal Soc.* **2014**, *39*, 1229–1237.
19. Bahaadini, M.; Hagan, P.C.; Mitra, R.; Khosravi, M.H. Experimental and numerical study of asperity degradation in the direct shear test. *Eng. Geol.* **2016**, *204*, 41–52. [\[CrossRef\]](#)

20. Zhou, K.F.; Liu, C.X.; Li, S.; Cheng, Y.H. Size effect on the rheological shear mechanical behaviors of different joints: A numerical study. *Geofluids* **2022**, *2022*, 1–9. [[CrossRef](#)]
21. Zhang, X.; Lin, H.; Wang, Y.X.; Yong, R.; Zhao, Y.L.; Du, S.G. Damage evolution characteristics of saw-tooth joint under shear creep condition. *Int. J. Damage Mech.* **2021**, *30*, 453–480. [[CrossRef](#)]
22. Jiang, M.J.; Liu, J.; Crosta, G.B.; Li, T. Dem analysis of the effect of joint geometry on the shear behavior of rocks. *Comptes Rendus Mécanique* **2017**, *345*, 779–796. [[CrossRef](#)]
23. Jiang, Y.J.; Zhang, S.H.; Luan, H.J.; Chen, L.J.; Zhang, G.C.; Wang, C.S. Numerical Investigation on the Effect of Cyclic Loading on Macro-meso Shear Characteristics of Rock Joints. *J. China Coal Soc.* **2022**, 1–13.
24. Bahaaddini, M.; Sharrock, G.; Hebblewhite, B.K. Numerical direct shear tests to model the shear behaviour of rock joints. *Comput. Geotech.* **2013**, *51*, 101–115. [[CrossRef](#)]
25. Yang, X.X.; Qiao, W.G. Numerical investigation of the shear behavior of granite materials containing discontinuous joints by utilizing the flat-joint model. *Comput. Geotech.* **2018**, *104*, 69–80. [[CrossRef](#)]
26. Tang, W.Y.; Lin, H. Influence of dentate discontinuity height on shear properties of soft structure plane. *J. Cent. South Univ. Sci. Technol.* **2017**, *48*, 1300–1307.
27. Xia, C.C.; Song, Y.L.; Tang, Z.C.; Song, Y.J.; Shou, C. Particle flow numerical simulation for shear behavior of rough joints. *Chin. J. Rock Mech. Eng.* **2012**, *31*, 1545–1552.
28. Liu, X.R.; Xu, B.; Huang, J.H.; Lin, G.Y.; Zhou, X.H.; Wang, J.W.; Xiong, F. Macro-meso shear mechanical behaviors of coalescent rock joints with different morphologies. *Chin. J. Geotech. Eng.* **2021**, *43*, 406–415.
29. Cao, R.H.; Cao, P.; Lin, H.; Ma, G.W.; Zhang, C.Y.; Jiang, C. Failure characteristics of jointed rock-like material containing multi-joints under a compressive-shear test: Experimental and numerical analyses. *Arch. Civ. Mech. Eng.* **2018**, *18*, 784–798. [[CrossRef](#)]
30. Wang, X.; Zhang, X.Z.; Zhu, C.Q.; Meng, Q.S. Shear tests of interfaces between calcareous sand and steel. *Mar. Georesour. Geotechnol.* **2018**, *37*, 1095–1104. [[CrossRef](#)]
31. Jiang, Q.; Song, L.B. Application and prospect of 3D printing technology to physical modeling in rock mechanics. *Chin. J. Rock Mech. Eng.* **2018**, *37*, 23–37.
32. Wang, C.S.; Jiang, Y.J.; Wang, G.; Luan, H.J.; Zhang, Y.C.; Zhang, S.H. Experimental investigation on the shear behavior of the bolt-grout interface under CNL and CNS conditions considering realistic bolt profiles. *Geomech. Geophys. Geo-Energy Geo-Resour.* **2022**, *8*, 1–23. [[CrossRef](#)]
33. Tian, W.; Pei, Z.R.; Han, N. A preliminary research on three-dimensional reconstruction and mechanical characteristics of rock mass based on CT scanning and 3D printing technology. *Rock Soil Mech.* **2017**, *38*, 2297–2305.
34. Cui, J.G.; Zhang, C.Q.; Liu, L.P.; Zhou, H.; Cheng, G.T. Study of effect of shear velocity on mechanical characteristics of bolt-grout interface. *Rock Soil Mech.* **2018**, *39*, 275–281.
35. Park, J.W.; Song, J.J. Numerical simulation of a direct shear test on a rock joint using a bonded-particle model. *Int. J. Rock Mech. Min.* **2009**, *46*, 1315–1328. [[CrossRef](#)]
36. Liu, X.R.; Deng, Z.Y.; Liu, Y.Q.; Lu, Y.M.; Liu, S.L.; Han, Y.F. Macroscopic and microscopic analysis of particle flow in pre-peak cyclic direct shear test of rock joint. *J. China Coal Soc.* **2019**, *44*, 2103–2115.
37. Wang, X.; Wang, X.Z.; Shen, J.H.; Zhu, C.Q. Particle size and confining-pressure effects of shear characteristics of coral sand: An experimental study. *Bull. Eng. Geol. Environ.* **2022**, *81*, 97. [[CrossRef](#)]
38. Dong, L.; Zhang, H.; Lv, J.S.; Shi, R.M. Rock cutting characteristics with single pick and prediction of cutting force based on force chain. *Rock Soil Mech.* **2022**, *43*, 3036–3046.

Disclaimer/Publisher’s Note: The statements, opinions and data contained in all publications are solely those of the individual author(s) and contributor(s) and not of MDPI and/or the editor(s). MDPI and/or the editor(s) disclaim responsibility for any injury to people or property resulting from any ideas, methods, instructions or products referred to in the content.